

Effect of *A*-site and *B*-site substitution on the infrared reflectivity spectra of $\text{La}_{1-y}\text{A}_y\text{Mn}_{1-x}\text{B}_x\text{O}_3$ ($\text{A} = \text{Ba, Sr}$; $\text{B} = \text{Cu, Zn, Sc}$; $0 < y \leq 0.3$; $0 \leq x \leq 0.1$) manganites

G. De Marzi,¹ Z. V. Popović,^{1,2} A. Cantarero,¹ Z. Dohčević-Mitrović,² N. Paunović,² J. Bok,³ and F. Sapiña¹¹Materials Science Institute, University of Valencia, P.O. Box 22085, 46071 Valencia, Spain²Institute of Physics, P.O. Box 68, 11080 Belgrade, Serbia³Solid State Physics Laboratory, ESPCI-UPR5 CNRS, 75005 Paris, France

(Received 10 December 2002; revised manuscript received 21 February 2003; published 7 August 2003)

We have measured the infrared reflectivity spectra of $\text{La}_{1-y}[\text{Sr}(\text{Ba})]_y\text{Mn}_{1-x}[\text{Cu}(\text{Zn}, \text{Sc})]_x\text{O}_3$ ($0 < y \leq 0.3$, $0 \leq x \leq 0.10$) manganites, in a wide frequency ($100\text{--}4000\text{ cm}^{-1}$) and temperature ($80\text{ K--}300\text{ K}$) range. The reflectivity spectra were analyzed by a fitting procedure based on a model that includes Drude, midinfrared electronic, and phonon oscillator contributions to the dielectric constant. Six infrared active ($3A_u$ and $3E_u$) modes of rhombohedral symmetry are clearly observed. We assigned all observed modes according to existing lattice dynamical calculations for the rhombohedral structure of LaMnO_3 . A decrease of the rhombohedral distortion below the paramagnetic-ferromagnetic transition is manifested through a lowering or complete removal of the frequency difference between the A_u and E_u modes.

DOI: 10.1103/PhysRevB.68.064302

PACS number(s): 78.30.Hv, 75.47.Lx, 63.20.Dj, 78.20.-e

I. INTRODUCTION

During the last decade $R_{1-x}A_x\text{MnO}_3$ pseudocubic manganites (R is a rare-earth metal, La, Pr, Nd, Dy; A is an alkaline-earth metal, Sr, Ca, Ba, Pb) have attracted much attention because of their intriguing physical properties that make these systems promising for applications as magnetic sensors. The phase diagram of these compounds is complex, and many variables such as pressure,¹ applied magnetic field,^{2,3} temperature,^{2,4} and A -site average ionic radius⁵ determine a wide range of ground states in the system. The most interesting property of these systems is the colossal magnetoresistance, which occurs near the Curie temperature T_C , when the system undergoes a transition from the paramagnetic (PM) to the ferromagnetic (FM) state. Ferromagnetism in these systems has been usually explained in terms of the “double exchange” (DE) model proposed by Zener.⁶ In the framework of the DE model, the e_g antibonding electrons can hop between neighboring Mn ions with different valence when their core spins are ferromagnetically coupled, but the spin disorder prevents such hopping processes above T_C . Further studies on these materials have shown that other mechanisms influence the phase transitions, among them the electron-phonon interaction arising from the Jahn-Teller (JT) distortions,⁷ the orbital polarization,⁸ the electron-electron correlations, and the coupling between spin and orbital structure.⁹

Studies of $R_{1-x}A_x\text{MnO}_3$ with x close to 0.30 have shown the existence of a correlation between T_C and the tolerance factor t ($t = d_{A-O} / \sqrt{2}d_{B-O}$, where d_{A-O} and d_{B-O} are the A -O and B -O bond lengths) of the perovskite structure ABO_3 ,¹⁰ or the mean size of cations $\langle r_A \rangle$ at the A site.¹⁰⁻¹² It is found that the lattice distortion is large in the PM phase (above T_C), but it decreases significantly in the FM phase. This means that the MnO_6 octahedra are highly distorted for $T > T_C$ but the magnitude of this distortion decreases as T approaches T_C . The idea is that a PM-FM transition can occur more easily if the octahedra are undistorted and the

Mn-O-Mn angles tend to be 180° .¹⁰ This can be obtained, for example, by changing the average dimension of the atom at the A and/or B site. Regarding the B cationic sublattice, attention has been paid to the B -site substitutions on the charge-ordered ground state (i.e., 50% Mn^{4+}),¹³ but there are few results concerning Mn substitution having the optimum content of Mn^{4+} (ca. 30%).¹²

Substitution of atoms in specific sites in the lattice affects the vibrational properties of the host material through the mass, the bonding strength, and the bonding configuration changes. Thus, vibrational spectroscopy (Raman and infrared) is a very effective tool for studying the role of A - and B -site substitution in manganites. Moreover, infrared spectroscopy is particularly useful for systems where lattice and electrons are strongly coupled (electron-phonon interaction). Having this in mind we have measured the reflectivity spectra of polycrystalline $\text{La}_{1-y}[\text{Sr}(\text{Ba})]_y\text{Mn}_{1-x}\text{B}_x\text{O}_3$ ($B = \text{Cu, Zn, Sc}$) samples. The values of y and x doping, together with the Curie temperature (T_C) of all investigated samples are given in Table I. The values of T_C of these compounds appear clearly related to the mean size of cations at B sites. In fact, in the case of large Mn substitutional defects, El-Fadli *et al.*¹² have found that the decrease in T_C associated with the increase in x is mainly determined by the local effect of the structural disorder introduced by large substitutional cations, and it is poorly modulated by the magnetic nature of the substitutional metals (Cu^{2+} versus Zn^{2+} and Sc^{3+}) or by the different stoichiometries of the samples (Sc^{3+} versus Cu^{2+} and Zn^{2+}). This fact has been interpreted by considering the variation of the electronic contribution to T_C with the structural disorder introduced by the presence of cations with different sizes at B sites. For more details, see Ref. 12.

The B -free end member of the series, $\text{La}_{0.7}\text{Sr}_{0.3}\text{MnO}_3$, has been extensively studied with a great variety of techniques; regarding the spectroscopic spectra, see, for example, optical conductivity measurements¹⁴⁻¹⁶ and Raman scattering.¹⁷⁻²⁰ However, reflectivity spectra of $\text{La}_{1-y}\text{A}_y\text{Mn}_{1-x}\text{B}_x\text{O}_3$, to the

TABLE I. Chemical analysis and the Curie temperatures T_C (K) for samples with the nominal composition $\text{La}_{1-y}\text{A}_y\text{Mn}_{1-x}\text{B}_x\text{O}_{3+\delta}$. Estimated errors in the La:Mn ratios are 0.01; the estimated error in Mn^{4+} (%) is $\pm 1\%$ (Ref. 12).

x	0.00	0.02	0.04	0.06	0.08	0.10
$A = \text{Sr}; B = \text{Cu}$						
y	0.30	0.274	0.248	0.222	0.196	0.170
Mn^{4+} (%)	31	32	32	32	35	32
δ	0.005	0.010	0.010	0.010	0.023	0.010
T_c	372	358	331	308	274	236
$A = \text{Sr}; B = \text{Zn}$						
y		0.274	0.248	0.222	0.196	0.170
Mn^{4+} (%)		30	31	33	32	33
δ		0	0.005	0.014	0.010	0.014
T_c		350	326	284	233	179
$A = \text{Ba}; B = \text{Cu}$						
y	0.30	0.274	0.248	0.222	0.196	0.170
Mn^{4+} (%)	31	31	31	33	30	32
δ	0.005	0.005	0.005	0.014	0	0.010
T_c	330	318	296	260	221	183
$A = \text{Ba}; B = \text{Sc}$						
y		0.294	0.288	0.282	0.276	0.270
Mn^{4+} (%)		31	30	31	31	32
δ		0.005	0	0.005	0.005	0.010
T_c		296	258	216	184	168

best of our knowledge, have not been published yet.

In this paper we present the infrared reflectivity spectra of four series samples of $\text{La}_{1-y}\text{Sr}_y\text{Mn}_{1-x}\text{B}_x\text{O}_3$ (with $B = \text{Cu}, \text{Zn}$), and $\text{La}_{1-y}\text{Ba}_y\text{Mn}_{1-x}\text{B}_x\text{O}_3$ (with $B = \text{Cu}, \text{Sc}$). The concentration of B ions was $x = 0.00, 0.02, 0.04, 0.06, 0.08$, and 0.10 , giving a total of 22 samples investigated. Because the optimum doping (the minimum vacancies at the A and the B sites, the strongest colossal magnetoresistance effect) is realized for concentration of Mn^{4+} ions of about 30%, we kept this value ($[\text{Mn}^{4+}]/([\text{Mn}^{4+}] + [\text{Mn}^{3+}]) \sim 0.30 \pm 0.02$) through the whole series by varying the Sr or Ba concentration y . We assigned all observed infrared active modes according to the lattice dynamical calculation for rhombohedral symmetry of LaMnO_3 . We found that the strongest (smallest) rhombohedral distortion, from spectroscopic reasons, exists in the case of the $\text{La}_{0.87}\text{Sr}_{0.17}\text{Mn}_{0.9}\text{Zn}_{0.1}\text{O}_3$ ($\text{La}_{0.73}\text{Ba}_{0.17}\text{Mn}_{0.9}\text{Sc}_{0.1}\text{O}_3$) sample. By lowering temperature we found in the $\text{La}_{0.87}\text{Sr}_{0.17}\text{Mn}_{0.9}\text{Zn}_{0.1}\text{O}_3$ sample that (1) the lowest-frequency A_u^1 ($\omega_{TO} = 144 \text{ cm}^{-1}$) and E_u^1 ($\omega_{TO} = 166 \text{ cm}^{-1}$) modes merge into one mode at temperatures below the Curie temperature of 179 K; (2) the oscillator strength of the second oscillator of the A_u^2 symmetry rapidly increases by lowering the temperature; (3) the highest-frequency mode pair softens remarkably at the phase transition. These findings are a clear indication that the structure distortion is strongly reduced when these oxides undergo a phase transition from the paramagnetic into the ferromagnetic state.

II. EXPERIMENT

Single-phase $\text{La}_{1-y}[\text{Sr}(\text{Ba})]_y\text{Mn}_{1-x}\text{B}_x\text{O}_3$ ($B = \text{Cu}, \text{Zn}, \text{Sc}$) samples have been prepared via the acetic acid

solution freeze-drying method. This soft procedure makes possible strict stoichiometric control, and the synthetic variables allow one to maintain a constant proportion of Mn^{4+} (ca. 30%) in the 22 compounds prepared. In this way, the concentration of cationic vacancies at A and B sites is practically negligible in all cases. X-ray powder diffraction patterns corresponding to the 22 compounds have been completely indexed and refined with rhombohedral perovskite symmetry and the $R\bar{3}c$ space group. Details on the preparation of the studied samples, together with x-ray diffraction and magnetization measurements, have been published elsewhere.¹² Disk-shaped pellets were optically polished using diamond paste. The size of the diamond grains was less than $0.5 \mu\text{m}$.

Reflectivity spectra were measured with a BOMEM DA-8 spectrometer. A deuterated triglycine sulfate (DTGS) pyroelectric detector was used to cover the wave-number region from 80 to 600 cm^{-1} ; a liquid-nitrogen-cooled Hg-Cd-Te detector was used from 500 to 5000 cm^{-1} . Spectra were collected with 2 cm^{-1} resolution, with 1000 interferograms added for each spectrum. For low-temperature measurements a Janis Super Tran (ST-100) continuous flow cryostat was used. As reference mirror we used an evaporated Au film.

III. RESULTS AND DISCUSSION

Figure 1 shows the room temperature reflectivity spectra of $\text{La}_{1-y}[\text{Sr}(\text{Ba})]_y\text{Mn}_{1-x}\text{B}_x\text{O}_3$ ($B = \text{Cu}, \text{Zn}, \text{Sc}$) polycrystalline samples in the spectral range from 80 to 4000 cm^{-1} . The common features presented in the four panels of Fig. 1 are three strong phonon bands, a wide structure centered at

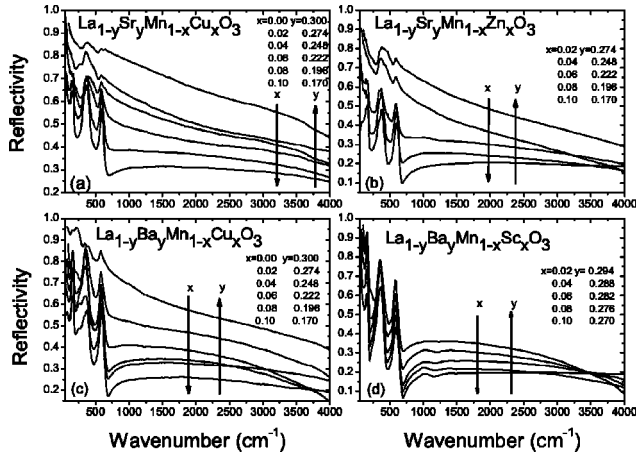


FIG. 1. Room temperature reflectivity spectra of $\text{La}_{1-y}[\text{Sr}(\text{Ba})]_y\text{Mn}_{1-x}[\text{Cu}(\text{Zn},\text{Sc})]_x\text{O}_3$ polycrystalline samples in the $80\text{--}4000\text{ cm}^{-1}$ spectral range.

about 2000 cm^{-1} , and a free carrier contribution to the reflectivity spectra. In $\text{La}_{0.7}\text{Sr}_{0.3}\text{MnO}_3$ [Fig. 1(a)] and $\text{La}_{0.7}\text{Ba}_{0.3}\text{MnO}_3$ [Fig. 1(c)] the reststrahlen oscillators are masked by a Drude-like background that can be attributed to the mobile holes introduced by Sr or Ba doping. By comparison of the $\text{La}_{0.7}\text{Sr}_{0.3}\text{MnO}_3$ reflectivity spectra [Fig. 1(a)] with the corresponding single crystal data¹⁶ at frequencies below 20 meV (where influence of deterioration of the sample surface by polishing on the reflectivity spectra was not observed), we found that our spectra are less reflective for only 3%. This means that the scattering losses at the polished surface of our samples were reasonably small.

When B ions are introduced in the Mn sites of the system, the Drude tail gradually decreases by increasing x and the phonon peaks become fully pronounced for the highest concentration of B-ion dopants. Figure 2 shows the reflectivity spectra of four samples with the highest doping level ($x = 0.1$). In that case, the influence of free carriers on the phonon dynamic is strongly reduced, allowing a more detailed analysis of the phonon spectra. Due to the insulating behavior of these samples, the damage of the sample surface by polishing has negligible influence on the reflectivity spectra; see Ref. 16. These spectra were analyzed both by a Kramers-Kronig analysis (KKA) and by the numerical fitting of reflectivity data. The values of transverse optical (TO) frequencies, obtained from KKA as frequency position of the optical conductivity maxima, are introduced as starting parameter in a “classical-oscillator model,” defined via the expression

$$\tilde{\epsilon}(\omega) = \epsilon_\infty + \sum_{j=1}^5 \frac{S_j^2}{\omega_{TO,j}^2 - \omega^2 - i\omega\gamma_{TO,j}} - \frac{\Omega_p^2}{\omega(\omega + i\gamma_p)} + \frac{S_{MIR}^2}{\omega_{MIR}^2 - \omega^2 - i\omega\gamma_{MIR}}, \quad (1)$$

where ω_{TO_j} and γ_{TO_j} are the TO mode frequency and line-width of the j th oscillator, S_j is the oscillator strength, and Ω_p and γ_p are the plasma frequency and damping, respec-

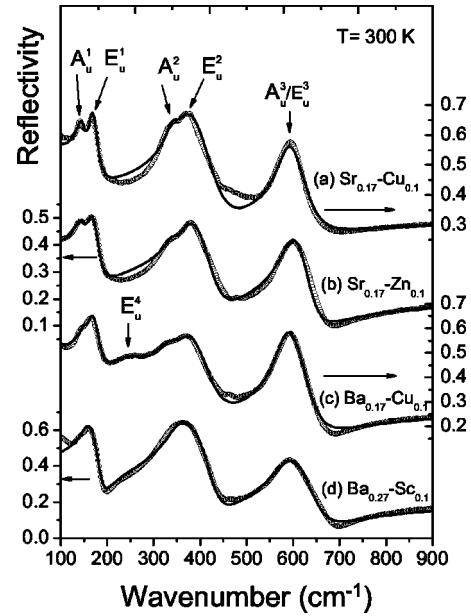


FIG. 2. Room temperature reflectivity spectra of $\text{La}_{1-y}[\text{Sr}(\text{Ba})]_y\text{Mn}_{0.90}[\text{Cu}(\text{Zn},\text{Sc})]_{0.10}\text{O}_3$ samples in the $100\text{--}900\text{ cm}^{-1}$ spectral range. Experimental data are represented by circles; solid lines are calculated spectra. (a) $\text{La}_{0.83}\text{Sr}_{0.17}\text{Mn}_{0.90}\text{Cu}_{0.10}\text{O}_3$, (b) $\text{La}_{0.83}\text{Sr}_{0.17}\text{Mn}_{0.90}\text{Zn}_{0.10}\text{O}_3$, (c) $\text{La}_{0.83}\text{Ba}_{0.17}\text{Mn}_{0.90}\text{Cu}_{0.10}\text{O}_3$, and (d) $\text{La}_{0.73}\text{Ba}_{0.27}\text{Mn}_{0.90}\text{Sc}_{0.10}\text{O}_3$.

tively. The third term in Eq. (1) describes the midinfrared (MIR) contribution to the dielectric constant due to the polaron absorption in these systems. The best fit parameters are listed in Table II. As can be seen from Fig. 2, the agreement between observed (open circles) and calculated reflectivity spectra (solid lines) is very good.

According to Fig. 2 and Table II, six infrared active modes with TO-mode frequencies around 144, 166, 266, 340, 370, and 590 cm^{-1} are observed. We assigned these modes with the help of the lattice-dynamical calculation for rhombohedral LaMnO_3 .²¹

In the ideal cubic perovskite ABO_3 there are 3 ir active modes of the F_{1u} symmetry at the Γ point of the Brillouin zone.²⁰ The lowest-frequency F_{1u} mode (the external mode) corresponds to the vibration of the A ions against the BO_6 octahedra, the bending mode (intermediate-frequency F_{1u} mode) corresponds to a modulation of the Mn–O–Mn angle, whereas the highest-frequency F_{1u} mode originates from Mn–O bond stretching vibrations of the MnO_6 octahedra. Our samples exhibit rhombohedral crystal structure,¹² space group $D_{3d}^6(R\bar{3}c)$, $Z=2$. In this case eight modes ($3A_u + 5E_u$) are expected to be observed in the infrared spectra. As it is discussed in Ref. 21, the $3A_u$ and three out of five E_u modes arise from the removal of degeneracy of the triply degenerate F_{1u} modes of the ideal cubic perovskite structure. Since the rhombohedral distortion is weak, the frequency splitting between the corresponding A_u and E_u modes is expected to be small. Because of that the A_u modes have not been resolved from the E_u ones in a previously published infrared reflectivity spectra of rhombohedral LaMnO_3 .²¹

In Fig. 2 we observe two mode doublets with TO frequen-

TABLE II. Optical parameters (in cm^{-1}) used to fit the reflectivity spectra of $\text{La}_{1-y}\text{A}_y\text{Mn}_{0.9}\text{B}_{0.1}\text{O}_3$. $y=0.17$ for $A=\text{Sr}, \text{Ba}$ and $B=\text{Cu}, \text{Zn}$; $y=0.27$ for $A=\text{Ba}$, $B=\text{Sc}$.

$A-B$	Sr-Cu	Sr-Zn	Ba-Cu	Ba-Sc
ϵ_∞	6.1	6.73	7.68	7.54
Ω_p	3956	1087	1293	
γ_D	5920	1377	842	
S_1	301	208	221	440
γ_1	20	28	20	29
ω_1	144	144	150	155
S_2	300	223	342	
γ_2	15	23	21	
ω_2	166	166	166	
S_3			512	
γ_3			109	
ω_3			266	
S_4	489	201	446	825
γ_4	30	35	60	52
ω_4	340	341	335	346
S_5	812	556	596	
γ_5	50	55	67	
ω_5	365	374	363.5	
S_6	741	570	734	651
γ_6	46	50	40	65
ω_6	584	593	578	581
S_{MIR}	7600	2275	5487	
Γ_{MIR}	4324	1729	4025	
ω_{MIR}	3193	2875	2916	

cies at about 144/166 and 340/375 cm^{-1} , and a single mode at about 590 cm^{-1} . The doublets can be assigned as the A_u - E_u mode pairs. The frequencies of the A_u and the corresponding E_u modes differ about $E_u^{1(2)} - A_u^{1(2)} = 22 \text{ cm}^{-1}$ (29 cm^{-1}), which is in good agreement with the theoretical predictions of 18 cm^{-1} (47 cm^{-1}).²¹ In the case of the 590 cm^{-1} mode, the lattice dynamical calculation predicts almost the same frequency for the A_u and the E_u modes

($E_u^3 - A_u^3 = 1 \text{ cm}^{-1}$). Because of that no A_u - E_u splitting is observed in the infrared spectra (Fig. 2) for these bond stretching modes.

Figure 3 depicts the ionic displacement patterns of all infrared ($3A_u + 5E_u$) active modes obtained by a shell model calculations.²¹ According to Fig. 3, the lowest-frequency phonon modes of A_u ($\omega_{TO}^{calc} = 162 \text{ cm}^{-1}$) and E_u ($\omega_{TO}^{calc} = 180 \text{ cm}^{-1}$) symmetry originate from the La ions vibration against the MnO_6 octahedra along the z and $y(x)$ axis, respectively. These modes are very sensitive to the rhombohedral distortion. In the case of $\text{La}_{1-y}\text{Sr}_y\text{Mn}_{1-x}\text{B}_x\text{O}_3$ ($B = \text{Cu}, \text{Zn}$), Figs. 2(a) and 2(b), the A_u^1 and E_u^1 modes are clearly resolved at 144 and 166 cm^{-1} (Table II). In the $\text{La}_{1-y}\text{Ba}_y\text{Mn}_{1-x}\text{B}_x\text{O}_3$ ($B = \text{Cu}, \text{Sc}$) samples it was difficult to resolve A_u^1 from E_u^1 for $B = \text{Cu}$ [Fig. 2(c)], and completely impossible in the case of $B = \text{Sc}$ [Fig. 2(d)]. Since the frequency separation for a given pair of A_u - E_u modes is a measure of the deviation of the structure from the ideal (cubic) one, we concluded that Ba produces less distortion than Sr. It can be expected because the Ba atoms are very close in size and weight to the La atoms.

The next doublet of A_u^2 and E_u^2 modes represents bond bending O-Mn-O vibrations. The calculated frequencies at 310 cm^{-1} and 357 cm^{-1} are close to the experimental values of 340 cm^{-1} and 370 cm^{-1} , respectively. These modes should be sensitive to the PM-FM phase transition also, because the DE interaction modulates the Mn-O-Mn angle and consequently can induce some phonon frequency and broadening change. As we already mentioned the A_u^3 - E_u^3 mode doublet appears as one degenerate mode in the infrared spectra, which is in agreement with lattice dynamical calculation.²¹ The E_u^4 mode in the rhombohedral phase represents the torsional oxygen vibrations of the oxygen octahedra [$\omega_{TO}^{calc}(E_u^4) = 240 \text{ cm}^{-1}$; Fig. 3]. The fact that this mode is inactive in the parent cubic structure and since the distortion of rhombohedral materials is small, the corresponding band in the ir spectra of rhombohedral perovskites should be relatively weak. Actually, we clearly observe one additional mode at about 266 cm^{-1} [Fig. 2(c), Table II], only in the case of the $\text{Ba}_{0.17}\text{Cu}_{0.1}$ sample. The E_u^5 mode (Fig. 3), which

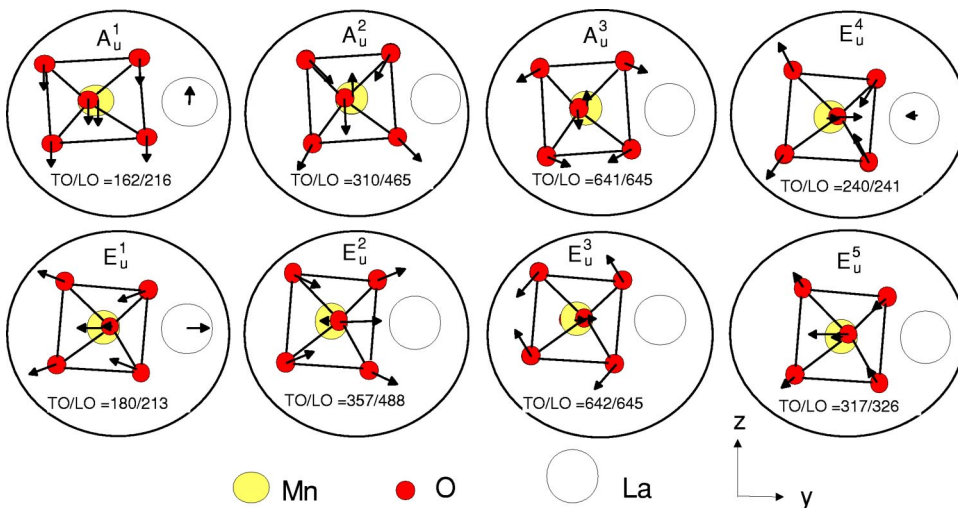


FIG. 3. Ionic displacement patterns of the A_u and the E_u symmetry infrared active modes in rhombohedral LaMnO_3 . TO/LO mode frequencies (in cm^{-1}) are taken from Ref. 21.

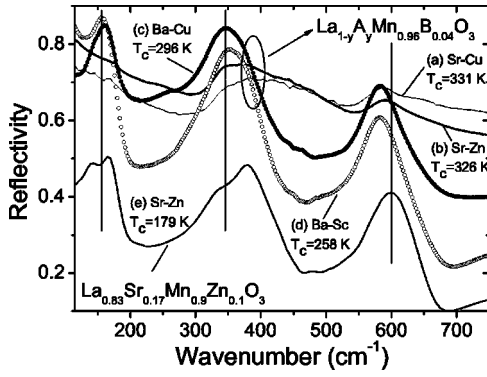


FIG. 4. Reflectivity spectra of $\text{La}_{1-y}\text{A}_y\text{Mn}_{0.96}\text{B}_{0.04}\text{O}_3$ samples at room temperature. (a) $A\text{-B}=\text{Sr-Cu}$, $y=0.248$; (b) $A\text{-B}=\text{Sr-Zn}$, $y=0.248$; (c) $A\text{-B}=\text{Ba-Cu}$, $y=0.248$; (d) $A\text{-B}=\text{Ba-Sc}$, $y=0.288$. (e) Reflectivity spectra of $\text{La}_{0.83}\text{Sr}_{0.17}\text{Mn}_{0.9}\text{Zn}_{0.1}\text{O}_3$ samples. T_C denotes the Curie temperature.

involves predominantly the motions of Mn ions, is not registered in our spectra. The calculated frequency of this mode ($\omega_{TO}^{calc}=317\text{ cm}^{-1}$) is inside the frequency range of the $A_u^2-E_u^2$ mode pair. Because of that one can expect an overlap of this mode with the middle-frequency bond bending modes.

Figures 4(a)–4(d) shows room temperature infrared reflectivity spectra of the 4% B -dopant concentration samples. These samples have a Curie temperature (see Table I) somewhat above or close to room temperature. Samples (a) and (b) in Fig. 4 are already in the metallic phase at room temperature, and consequently the free carriers mask the phonon structure in the infrared reflectivity spectra. Because of that it was hardly possible to extract phonon frequencies of these samples. By lowering the temperature these samples become better metals only. Samples (c) and (d) in Fig. 4 show no splitting of modes even in the paramagnetic phase. This leads us to the conclusion that rhombohedral distortion is strongly suppressed in low- B -dopant concentration samples. By lowering of temperature these samples become metals (below T_C) and free carriers again screen phonon structure. The $\text{Sr}_{0.17}\text{Zn}_{0.1}$ sample [spectrum (d) in Fig. 4] undergoes the PM (insulator) to FM (insulator) transition at $T_C=179\text{ K}$, allowing us a more detailed analysis of the infrared reflectivity spectra in this sample in both the PM and the FM phases. As can be seen by comparison of the (a)–(d) with the (e) reflectivity spectra (Fig. 4), the rhombohedral distortion creates a splitting of external and bond bending modes and hardening of the bond-stretching mode in the PM phase of the $\text{Zn}_{0.1}$ sample. The x-ray diffraction study of the same samples shows explicitly that rhombohedral distortion increases continuously by an increase of B -site concentration (see Ref. 12 for supporting materials). Namely, the O–B–O angle decreases from 166.5° ($x=0$) to 163.6° for $x=10\%$ of Zn.

In order to check if rhombohedral distortion is suppressed in the FM phase we measured the infrared reflectivity spectra of the $\text{La}_{0.83}\text{Sr}_{0.17}\text{Mn}_{0.9}\text{Zn}_{0.1}\text{O}_3$ sample at different temperatures (Fig. 5). This sample has an insulatorlike electrical resistivity versus temperature dependence [Fig. 6(a)]. Consequently, the plasma frequency for this sample decreases by

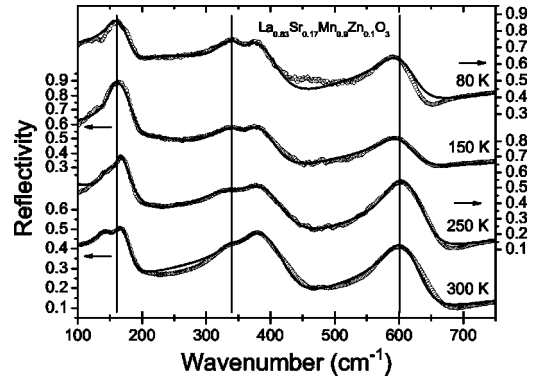


FIG. 5. Reflectivity spectra of $\text{La}_{0.83}\text{Sr}_{0.17}\text{Mn}_{0.9}\text{Zn}_{0.1}\text{O}_3$ samples at different temperatures. Experimental data are represented by circles; solid lines are calculated spectra.

lowering the temperature (see Table III). The frequency versus temperature dependencies for some of the observed infrared active modes are depicted in Figs. 6(b) and 6(c).

By lowering the temperature the lowest-frequency doublet seems to merge into one mode. The splitting of second doublet is not removed at the lowest temperature of 80 K applied in our experiment, but we found that the intensity of the 350 cm^{-1} oscillator (A_u^2 mode) rapidly increases by lowering the temperature. At 80 K this oscillator becomes stronger in intensity than the 370 cm^{-1} one (E_u^2). By further temperature decrease the A_u^2 oscillator should totally overwhelm the E_u^2 symmetry oscillator, and in a such way to remove the

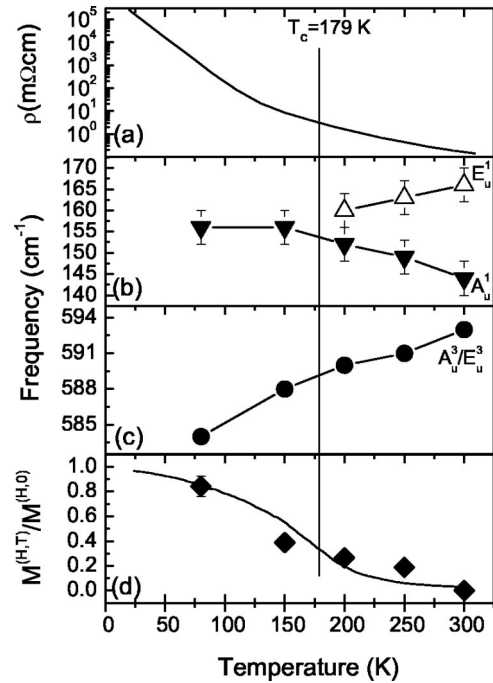


FIG. 6. (a) The specific electric resistivity vs temperature dependence of the $\text{La}_{0.83}\text{Sr}_{0.17}\text{Mn}_{0.9}\text{Zn}_{0.1}\text{O}_3$ sample. The frequency vs temperature dependence of the (b) $A_u^1-E_u^1$ and (c) $A_u^3-E_u^3$ mode pairs. (d) Reduced magnetization [$M(H,T)/M(H,0)$, $H=10\text{ kOe}$] vs temperature for the same sample. Points represent the normalized oscillator strength of the A_u^2 mode.

TABLE III. Optical parameters (in cm^{-1}) used to fit the reflectivity spectra of $\text{La}_{0.83}\text{Sr}_{0.17}\text{Mn}_{0.9}\text{Zn}_{0.1}\text{O}_3$ at different temperatures.

	Temperature (K)				
	300	250	200	150	80
ϵ_∞	6.73	7.92	8.5	8.9	8.89
Ω_p	1087	957	817	699	568
γ_D	1377	384	355	355	298
S_1	208	288	486	746	896
γ_1	28	20	13	10	19
ω_1	144	149	152	156	156
S_2	223	257	430		
γ_2	23	12	12		
ω_2	166	163	160		
S_3			956	856	1654
γ_3			198	203	238
ω_3			315	274	284
S_4	201	352	412	512	875
γ_4	35	41	35	42	35
ω_4	341	331	332	336	333
S_5	556	588	409	490	506
γ_5	55	61	32	45	33
ω_5	374	372	365	374	370
S_6	570	726	675	728	833
γ_6	50	47	45	55	36
ω_6	593	591	590	588	584
S_{MIR}	2275	4230	3985	7368	9889
Γ_{MIR}	1729	4123	3200	3325	2915
ω_{MIR}	2875	2896	2256	2245	2148

mode splitting of the second mode doublet (as it is the case of the $B_{0.04}$ samples, Fig. 4). We believe that the oscillator strength increase of the A_u^2 mode is spin-related. Namely, the DE interaction modulates the Mn–O–Mn angle and consequently changes the force constant of the A_u^2 bond bending normal mode. In Fig. 6(d) we compare the normalized strength (points) of the A_u^2 oscillator (Table III) with the normalized magnetization spectra (solid line).¹² As can be seen from Fig. 6(d) the A_u^2 mode oscillator strength maps well the normalized magnetization curve, indicating the spin-related behavior of the A_u^2 mode.

The $A_u^3-E_u^3$ mode doublet of the $\text{La}_{0.83}\text{Sr}_{0.17}\text{Mn}_{0.9}\text{Zn}_{0.1}\text{O}_3$ sample softens by lowering the temperature, spatially close to the phase transition, Fig. 6(c). The damping of phonons decreases by lowering the temperature (Table III), indicating that the lattice instability is lifted in the FM phase also. Thus, phonons contribute substantially to the phase transition. All these findings are a strong indication that the rhombohedral distortion is drastically reduced when the system undergoes the phase transition from the paramagnetic into the ferromagnetic state.

In conclusion, we have measured reflectivity spectra of $\text{La}_{1-y}[\text{Sr}(\text{Ba})]_y\text{Mn}_{1-x}[\text{Cu}(\text{Zn},\text{Sc})]_x\text{O}_3$ samples in the 80–4000 cm^{-1} range. We observed and assigned six of eight infrared active modes, predicted by factor-group analysis for rhombohedral symmetry of LaMnO_3 . The rhombohedral distortion-induced phonon doublet structure is clearly resolved for the lowest- (external) and the middle- (bond bending) frequency bands, whereas for the highest-frequency (bond stretching) band, only one mode is observed. These findings are fully in agreement with the lattice dynamical calculation of Abrashev *et al.*²¹ By lowering the temperature, the rhombohedral distortion in the $\text{La}_{0.83}\text{Sr}_{0.17}\text{Mn}_{0.9}\text{Zn}_{0.1}\text{O}_3$ sample is drastically reduced when the system undergoes the phase transition from the paramagnetic into the ferromagnetic phase. Consequently, the $A_u^1-E_u^1$ mode pair merges into one mode, whereas the bond stretching doublet at about 600 cm^{-1} softens for more than 10 cm^{-1} .

ACKNOWLEDGMENTS

One of us (Z.V.P.) thanks the Spain Ministry for Education, Culture and Sport for financial support. The authors would like to thank Dr V. N. Popov, who supplied us with the normal coordinates for infrared active modes of the rhombohedral LaMnO_3 . We acknowledge W. H. A. Thijssen for providing resistivity data prior to publication. This work was supported by the UE through a TMR grant (No. HPRN-CT2000-00021) and Serbian Ministry of Science and Technology under Project No. 1469.

¹H.Y. Hwang, T.T.M. Palstra, S-W. Cheong, and B. Batlogg, Phys. Rev. B **52**, 15 046 (1995).

²K.M. Kusters, J. Singleton, D.A. Keen, R. McGreevy, and W. Hayes, Physica B **155**, 362 (1989).

³R. von Helmolt, J. Wecker, B. Holzapfel, L. Schultz, and K. Samwer, Phys. Rev. Lett. **71**, 2331 (1993).

⁴G.M. Jonker and J.H. van Santen, Physica (Utrecht) **16**, 337 (1950).

⁵A.J. Millis, Nature (London) **392**, 147 (1998); J. Fontcuberta, Phys. World **12**, 33 (1999).

⁶Z. Zener, Phys. Rev. **82**, 403 (1951).

⁷A.J. Millis, P.B. Littlewood, and B.I. Shraiman, Phys. Rev. Lett. **74**, 5144 (1995).

⁸R. Maezono, S. Ishihara, and N. Nagaosa, Phys. Rev. B **57**, R13 993 (1998).

⁹S. Ishihara, J. Inoue, and S. Maekawa, Phys. Rev. B **55**, 8280 (1997).

¹⁰H.Y. Hwang, S-W. Cheong, P.G. Radaelli, M. Marezio, and B. Batlogg, Phys. Rev. Lett. **75**, 914 (1995); J. Fontcuberta, B. Martínez, A. Seffar, S. Piñol, J.L. García-Muñoz, and X. Obradors, *ibid.* **76**, 1122 (1996).

¹¹A. Maignan, V. Caignert, Ch. Simon, M. Hervieu, and B. Raveau,

- J. Mater. Chem. **5**, 1091 (1995); R. Mahesh, R. Mahendrian, A.K. Raychaudhuri, and C.N.R. Rao, J. Solid State Chem. **120**, 204 (1995).
- ¹²Z. El-Fadli, M. Redouane Metni, F. Sapiña, E. Martínez, J.V. Folgado, and A. Beltrán, Chem. Mater. **14**, 688 (2002). Tables of refined structural parameters for the rhombohedral setting are available free of charge at <http://pubs.acs.org>.
- ¹³A. Maignan, F. Damay, A. Barnabe, C. Martin, M. Hervieu, and B. Raveau, Philos. Trans. R. Soc. London, Ser. A **356**, 1635 (1998), and references therein.
- ¹⁴Y. Okimoto, T. Katsufuji, T. Ishikawa, T. Arima, and Y. Tokura, Phys. Rev. B **55**, 4206 (1997).
- ¹⁵M. Quijada, J. Černe, J.R. Simpson, H.D. Drew, K.H. Ahn, A.J. Millis, R. Shreekala, R. Ramesh, M. Rajeswari, and T. Venkatesan, Phys. Rev. B **58**, 16 093 (1998).
- ¹⁶K. Takenaka, K. Iida, Y. Sawaki, S. Sugai, Y. Morimoto, and A. Nakamura, J. Phys. Soc. Jpn. **68**, 1828 (1999).
- ¹⁷R. Gupta, A.K. Sood, R. Mahesh, and C.N.R. Rao, Phys. Rev. B **54**, 14 899 (1996).
- ¹⁸V.B. Podobedov, A. Weber, D.B. Romero, J.P. Rice, and H.D. Drew, Phys. Rev. B **58**, 43 (1998).
- ¹⁹V.A. Amelichev, B. Güttler, O.Yu. Gorbenco, A.R. Kaul, A.A. Bosak, and A.Yu. Ganin, Phys. Rev. B **63**, 104430 (2001).
- ²⁰E. Granado, N.O. Moreno, A. García, J.A. Sanjurjo, C. Rettori, I. Torriani, S.B. Oseroff, J.J. Neumeier, K.J. McClellan, S-W. Cheong, and Y. Tokura, Phys. Rev. B **58**, 11 435 (1998).
- ²¹M.V. Abrashev, A.P. Litvinchuk, M.N. Iliev, R.L. Meng, V.N. Popov, V.G. Ivanov, R.A. Chakalov, and C. Thomsen, Phys. Rev. B **59**, 4146 (1999).